Aluminosugilite and norrishite from the Funakozawa mine, Iwate Prefecture, Japan

Daisuke NISHIO-HAMANE[*], Mariko NAGASHIMA[**], Yuki MORI[***], Yoshiya OHKI[†] and Yasumitsu SUZUKI[‡]

[*]*Institute for Solid State Physics, the University of Tokyo, Kashiwa 277-8581, Japan*
[**]*Graduate School of Sciences and Technology for Innovation, Yamaguchi University, Yamaguchi 753-8512, Japan*
[***]*Diffraction and Scattering Division, Japan Synchrotron Radiation Research Institute, Sayo 679-5198, Japan*
[†]*Motoyoshida-cho, Mito, Ibaraki 310-0836, Japan*
[‡]*Miyata-cho, Hitachi, Ibaraki 317-0055, Japan*

Descriptive mineralogical studies, including single-crystal structure analysis, were conducted on aluminosugilite and norrishite, two rare minerals from the Funakozawa mine. Aluminosugilite occurs in the quartz layer spread along the schistosity of the slate as foliated reddish-light purple crystals up to 1 mm in diameter and 50 μm thick. The cleavage is indistinct, and the Mohs hardness is 6. Aluminosugilite coexists with aegirine and amphibole. In the outcrop, aluminosugilite often transforms into swinefordite with its texture retained. The representative chemical composition of aluminosugilite from a boulder sample was $K_{0.98}Na_{1.93}(Al_{1.31}Fe_{0.44}Mn_{0.17})_{\Sigma 1.91}Li_3Si_{12}O_{29.82}$, and single-crystal X-ray data yielded a hexagonal *P*6/*mcc* lattice with a = 9.9894(7) Å, c = 13.9527(9) Å, and V = 1205.77(14) Å^3. The structure refinement converged to R_1 = 2.67%. The structure may limit the accommodation of the Jahn-Teller cation, Mn^{3+}, due to symmetry. Norrishite is one of the most abundant constituent minerals in slate and coexists with aegirine and amphibole. In thin sections, norrishite is observed to be surrounded by quartz. Norrishite is brown to black and is in the form of irregularly shaped foil-like to plate-like crystals that exhibit perfect cleavage at {001} planes. Norrishite is also pleochroic and highly polychromatic with color variation from yellow to brown to green. The representative chemical composition of norrishite from a boulder was $K_{0.99}(Mn_{1.97}Mg_{0.09}Ti_{0.03}Li_{0.92})_{\Sigma 3}(Al_{0.22}Si_{3.78})_{\Sigma 4}O_{11.95}$, which represents an absolutely Fe-free composition. Single-crystal X-ray data yielded a monoclinic *C*2/*m* lattice with a = 5.3024(2) Å, b = 8.9520(4) Å, c = 10.0812(5) Å, β = 98.191(4)°, and V = 473.65(4) Å^3 as the 1*M* polytype. The structure refinement converged to R_1 = 4.30%. The structure is sufficiently flexible to accept the Jahn-Teller cation, Mn^{3+}, but then its ability to form a solid solution with other components is limited.

Keywords: Aluminosugilite, Norrishite, Funakozawa mine, Iwate Prefecture, Japan

INTRODUCTION

Sugilite is a member of the milarite group minerals first found in the Iwagi Islet, Ehime Prefecture, Japan, with an ideal formula of $KNa_2Fe_2^{3+}Li_3Si_{12}O_{30}$ (Kato et al., 1976; Murakami et al., 1976). Sugilite was one of the small constituent minerals of albitite in the Iwagi Islet, although it has been found in large quantities at the Wessels mine, the Kalahari manganese field, Republic of South Africa (Dunn et al., 1980). The sugilite crystals from the Wessels mine are characterized as bright violet to purple, while those from the Iwagi Islet are dull green. This extreme color variation has hindered the identification of sugilite; for example, purple sugilite from the Furumiya mine in Japan went unnoticed for a long time (Hirowatari and Fukuoka, 1988). Purple colored sugilite has also been found in manganese deposits such as at the Cerchiara mine (Italy) (Cabella et al., 1990), the Hoskins mine (Australia), the Woods mine (Australia) (Kawachi et al., 1994), and the Bruce mine (South Africa) (Moore et al., 2011), which typically contained small amounts of Mn. A more prominent feature has already been indicated by Kawachi et al. (1994) and Moore et al. (2011); according to the Al-Fe-Mn diagram, sugilite from several localities is dominated by Al rather than Fe and Mn. Aluminosugilite, an Al analogue of sugilite with an ideal formula of $KNa_2Al_2Li_3$

doi:10.2465/jmps.240509
D. Nishio-Hamane, hamane@issp.u-tokyo.ac.jp Corresponding author

$Si_{12}O_{30}$, was subsequently established by Nagashima et al. (2020) as a new mineral species from the Cerchiara mine.

Norrishite, a Li- and Mn-dominant oxymica with the ideal formula of $KLiMn_2^{3+}Si_4O_{10}O_2$, is found from localities where (alumino)sugilite occurs (e.g., Eggleton and Ashley, 1989; Tyrna and Guggenheim, 1991; Hawthorne et al., 1995; Gnos et al., 2003; Moore et al., 2011; Tomita et al., 2013; Oberti et al., 2016; Gu et al., 2019). Norrishite was once described as manganese biotite and was found in oxidized mineral assemblages typically associated with Na-Mn amphiboles. Eggleton and Ashley (1989) successfully established norrishite as a new mineral species from the Hoskins mine and pointed out the occurrence of a similar oxidized mineral assemblage from the Tanohata mine, the Kitakami Mountains, Japan, which was originally reported by Nambu et al. (1969).

The Funakozawa mine is one of the major manganese deposits in the Kitakami Mountains. This locality has been known for the occurrence of Li-bearing minerals exemplified by nambulite (Yoshii et al., 1972), and Mn-bearing ferri-leakeite as Na-Mn amphiboles (Nishio-Hamane et al., 2022). These occurrences suggest a similarity to the aforementioned oxidized mineral assemblages. The presence of so-called biotite has also been reported from this locality (e.g., Nambu, 1980), although the mineralogical characteristics were not investigated. Therefore, considering the mineral assemblages, further investigation is required. A recent study by Nishio-Hamane et al. (2023) finally identified this biotite as norrishite. Aluminosugilite was also observed in this locality (Nishio-Hamane et al., 2022).

This is a follow-up study of the brief report by Nishio-Hamane et al. (2022; 2023) to provide mineralogical data including structural analysis for aluminosugilite and norrishite using samples from the Funakozawa mine, Iwate Prefecture, Japan.

OCCURRENCE

The Funakozawa mine, Hirono Town, Iwate Prefecture (40°15′08″N 141°37′04″E) is included in the Rikuchu-Ono district situated at the northern margin of the Kitakami Mountains, Northeast Honshu, Japan (Yoshida et al., 1985). This district consists mainly of sedimentary rocks with Permian to Middle Mesozoic ages. The Funakozawa mine is a stratiform manganese deposit hosted in the Seki unit of the Iwaizumi belt. The surrounding area consists mainly of slate and chert that have been thermally metamorphosed by Cretaceous granitic bodies. According to the study of the stratiform manganese and manganiferous iron deposits in the Kitakami Mountains by Nambu (1980), the systematic mineralogical variation corresponds to the metamorphic grades of the country rocks, and four metamorphic grades were defined; the chlorite-, biotite-, cordierite-, and potassic feldspar zones. The Funakozawa mine is classified into the biotite zone (Nambu, 1980).

Our investigation began with boulders in the river. In 2017, the authors (Y.O. and Y.S.) found a boulder of slate containing aluminosugilite at the confluence of the Ono River, the main stream, and the Funakozawa River, a tributary (40°15′10″N 141°36′44″E). This was once the ore-dressing plant of the Funakozawa mine. The investigation was continued following the boulders and an outcrop of aluminosugilite was discovered near the old shaft of the Funakozawa mine, located upstream of the Funakozawa River. The outcrop is composed of slate with an almost vertical schistosity plane. The surface of the slate is blackened, but the interior is reddish in color due to the presence of amphiboles (mainly ferri-leakeite) as one of the main constituent minerals. Aluminosugilite with swinefordite (Li-rich member of the smectite group) occurs in thin layers beside the amphibole-bearing slate.

Other constituents in the slate are quartz, norrishite, braunite-neltnerite series minerals, and aegirine. Small amounts of albite, titanite, Mn-bearing diopside, and potassic-richterite are occasionally observed. The concentration and size of these constituent minerals significantly vary from layer to layer. For example, each major constituent mineral forms a dominant layer. The norrishite-dominant layer is fairly common in both outcrops and boulders. Marsturite and cerchiaraite-(Mn) are observed as veins crossing the layer of the braunite-neltnerite series minerals.

METHODS

Chemical analysis, single-crystal X-ray diffraction, and powder X-ray diffraction measurements were performed to characterize aluminosugilite and norrishite. Chemical analysis was conducted using a scanning electron microscope (JEOL IT-100) equipped with energy dispersive X-ray spectrometer at an accelerating voltage of 15 kV, a beam current of 0.8 nA, and a beam diameter of 1 μm at the Institute for Solid State Physics, the University of Tokyo. The ZAF method was used for data correction. $NaAlSi_3O_8$, MgO, Al_2O_3, $CaSiO_3$, $KTiPO_5$, Mn metal, and Fe metal were used as standards for Na, Mg, Al, Si, K, Ti, Mn, and Fe, respectively. Li_2O was estimated from the stoichiometry of each mineral.

Synchrotron powder X-ray diffraction patterns were collected using a large Debye-Scherrer camera equipped with MYTHEN detectors installed at the powder diffraction BL02B2 beamline of SPring-8, Hyogo, Japan (Kawa-

guchi et al., 2017). Rock samples were roughly crushed, and the target minerals were then selected. The mineral fragments were ground into a fine powder using an agate mortar and a pestle. Powder samples were packed into quartz glass capillaries with an outer diameter of 0.3 mm and a glass wall thickness of 0.01 mm. The wavelength of the incident X-rays was determined to be λ = 0.999393 Å using CeO_2 as a standard. Measurements were performed at room temperature (295 K) with an exposure time of 600 s.

Single-crystal X-ray diffraction analyses were conducted using a Rigaku XtaLAB Synergy-R/DW diffractometer equipped with a high-brightness X-ray source (PhotonJet-R/DW) and a hybrid photon counting (HPC) detector (HyPix-6000HE) installed at Yamaguchi University. The crystals were mounted on a glass fiber and intensity data were measured at room temperature using graphite-monochromatized Mo*K*α radiation (λ = 0.71073 Å). Empirical absorption correction using CrysAlis^{Pro} (Matsumoto et al., 2021) was applied. Structural refinement was performed with the SHELXL-2019/3 package (Sheldrick, 2015) using neutral scattering factors. Aluminosugilite contains Fe and Mn with similar X-ray scattering factors; therefore, the refinements were performed as Fe. The small amount of Al at *T* sites of the norrishite was also analyzed entirely as Si because the X-ray scattering factor for Al is indistinguishable from that for Si.

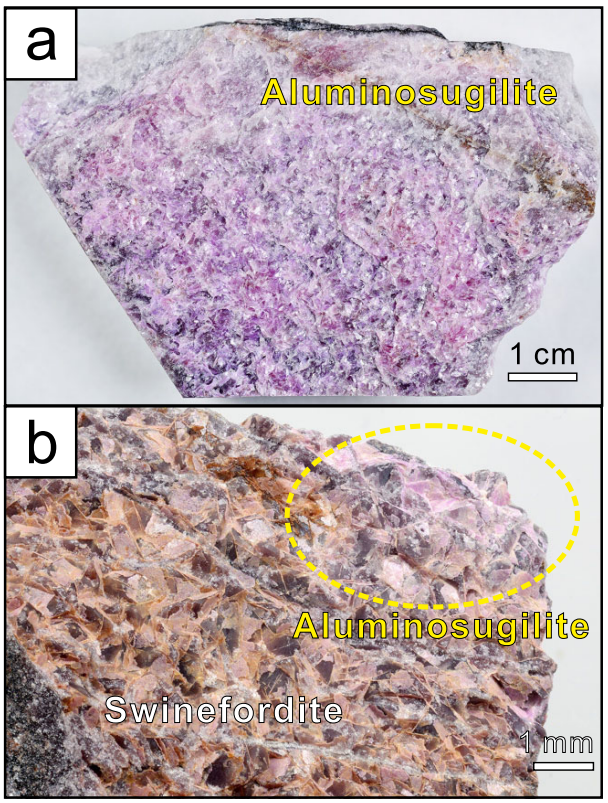

Figure 1. Aluminosugilite samples from (a) a boulder and (b) outcrop. Aluminosugilite obtained from the boulder is unaltered. Samples obtained from outcrops contain only a small amount of aluminosugilite, where most of the remaining aluminosugilite has been altered to swinefordite.

ALUMINOSUGILITE

Appearance

The boulder of slate found in 2017 was plate shaped with the longest side at 19 cm and a thickness of 5 cm. A partial specimen taken from this boulder is shown in Figure 1a. Aluminosugilite is concentrated in a thin quartz layer in the slate, so that a large number of foliated crystals of aluminosugilite were observed in the plane along that layer. The specimens obtained from the outcrop are shown in Figure 1b. Many foliated crystals were also observed in this specimen. However, most of these crystals had been altered to swinefordite (Suzuki, 2023), and only a small portion of aluminosugilite remained.

Figure 2 shows a cut section of the boulder sample. The thickness of the aluminosugilite-rich zone in the quartz layer is within 5 mm (Fig. 2a). Small amounts of aegirine and amphibole are also included in this aluminosugilite-rich zone (Fig. 2b). Aluminosugilite is a slightly reddish light purple and occurs as foliated crystals up to 1 mm in diameter and 50 μm thick. The crystals in this specimen are unaltered but often have holes filled with quartz (Fig. 2b). In thin section, the mineral is almost colorless with weak pleochroism.

Chemical composition

Two different specimens of aluminosugilite were obtained and separately prepared for chemical analysis. Table 1 summarizes the average chemical compositions of aluminosugilite. The empirical formulae were calculated on the basis of Si = 12 apfu, and the Li_2O wt% was recalculated as Li = 3 apfu. The representative chemical formulae of aluminosugilite are $K_{0.98}Na_{1.93}(Al_{1.31}Fe_{0.44}Mn_{0.17})_{\Sigma 1.91}Li_3Si_{12}O_{29.82}$ and $K_{0.95}Na_{1.99}(Al_{1.13}Fe_{0.51}Mn_{0.30})_{\Sigma 1.94}Li_3Si_{12}O_{29.88}$ from the boulder and the outcrop samples, respectively.

Figure 3 shows the compositional variation for the Al-Fe-Mn system. Although all analyzed points fall within the composition of aluminosugilite, the composition varies between samples. The composition of aluminosugilite in the boulder is plotted in a narrower range relative to those from outcrops. The aluminosugilite in the boulder is also characterized by a low Mn content below 10%, and an Al content in the 60-70% range. On the other hand, the composition of aluminosugilite from outcrops is rather broadly distributed with the Mn content more abundant

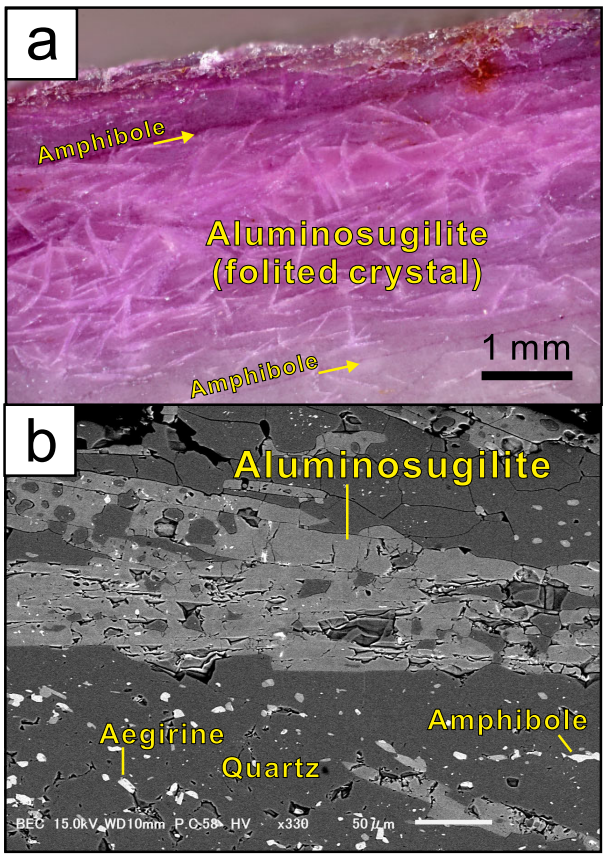

Figure 2. (a) Micrograph and (b) backscattered electron image of a section of aluminosugilite cut from a boulder.

Table 1. Chemical composition of aluminosugilite

	Boulder (n = 10)	Outcrop (n = 15)
	wt%	wt%
	Avg. (Min.-Max)	Avg. (Min.-Max)
K_2O	4.55 (4.19-4.88)	4.42 (4.08-4.83)
Na_2O	5.93 (5.46-6.41)	6.12 (5.67-6.60)
Al_2O_3	6.59 (6.03-7.87)	5.72 (4.29-6.95)
Fe_2O_3	3.47 (1.46-4.68)	4.02 (1.48-6.30)
Mn_2O_3	1.32 (0.78-1.85)	2.36 (1.56-3.29)
Li_2O^*	4.44	4.45
SiO_2	71.36 (70.35-72.47)	71.54 (69.64-73.48)
Total	97.66	98.63
	apfu	apfu
K	0.98	0.95
Na	1.93	1.99
Al	1.31	1.13
Fe	0.44	0.51
Mn	0.17	0.30
Σ	1.91	1.94
Li (fixed)	3	3
Si =	12	12
O	29.82	29.88

* Calculated value from stoichiometry.

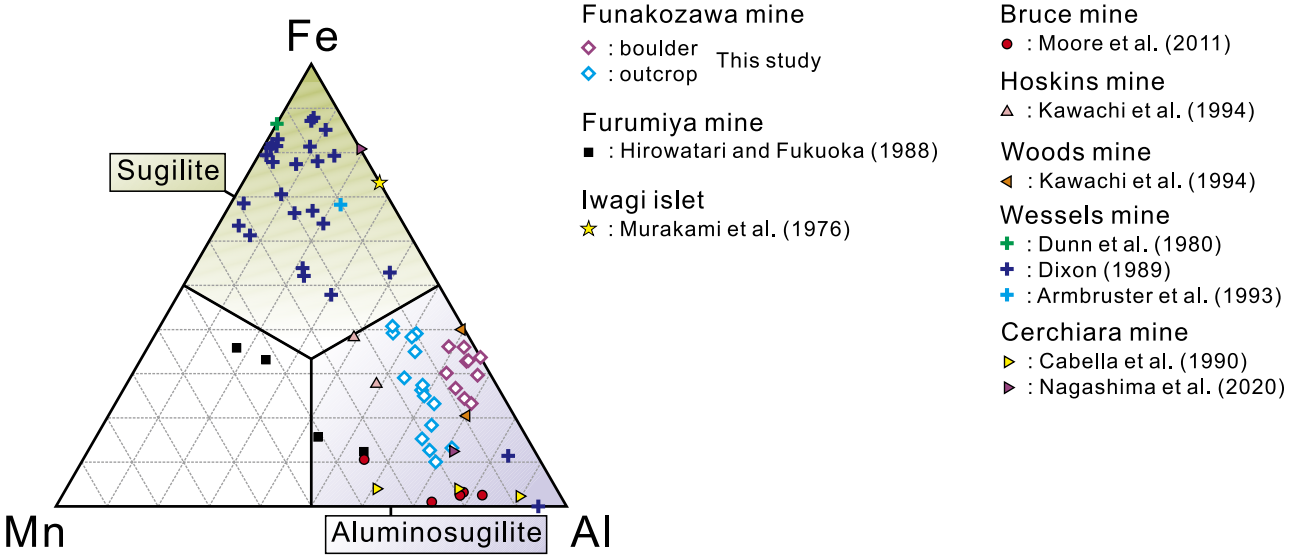

Figure 3. Compositional variation of aluminosugilite from the Funakozawa mine and sugilite series minerals from other localities.

at 10–20% than in the boulder samples. The range of Al content is even broader with variation from 45 to 70%. Therefore, the compositions of aluminosugilite from the boulder and outcrop samples did not overlap.

X-ray crystallography

Powder X-ray diffraction data were measured using the

Table 2. Experimental details of the single-crystal X-ray diffraction analysis

Sample	Aluminosugilite	Norrishite
Space group	*P*6/*mcc*	*C*2/*m*
Crystal size (mm)	0.11 × 0.08 × 0.04	0.57 × 0.24 × 0.08
Cell parameters	a = 9.9894(7) Å	a = 5.3024(2) Å
	c = 13.9527(9) Å	b = 8.9520(4) Å
	V = 1205.77(19) Å^3	c = 10.0812(5) Å
		β = 98.191(4)°
		V = 473.65(4) Å^3
Radiation	Mo$K\alpha$ (λ = 0.71073 Å)	
Monochromator	VariMax optics	
Diffractometer	RIGAKU HyPix-6000HE	
Scan type	ω scan	
Absorption correction	CrysAlis^{Pro} (Matsumoto et al., 2021)	
Refinement on F^2 using	SHELXL-2019/3	
θ min (°)	2.4	2.0
θ max (°)	36.3	40.6
Collected reflections	8184	4799
Unique reflections	1022	1563
Observed [$I > 2\sigma(I)$] reflections	786	1384
*R*int (%)	5.81	3.22
R_1 (%)	2.67	4.30
wR_2 (%)	7.97	13.11
S	1.07	1.14
No. of parameters	45	56
$\Delta\rho$max (e Å^{-3})	0.65	3.56
$\Delta\rho$min (e Å^{-3})	−0.47	−1.01

boulder sample because the sample volume was larger than that from the outcrop sample (Supplementary Fig. S1; Figs. S1 and S2 are available online from https://doi.org/10.2465/jmps.240509). Although a large amount of quartz was detected simultaneously, the diffraction peaks from aluminosugilite could be well identified, and the overall diffraction profile was very compatible with the milarite structure. A total of 49 peaks indexed in the d = 8.65–1.35 Å range were used to refine the unit cell parameters with the space group *P*6/*mcc*, which gave a = 9.9834(4) Å, c = 13.9669(8) Å, and V = 1207.00(11) Å^3. Supplementary Table S1 summarizes the powder X-ray diffraction data for aluminosugilite (Supplementary Tables S1 and S2 are available online from https://doi.org/10.2465/jmps.240509).

Structure refinement was conducted using the single-crystal X-ray diffraction data for the boulder sample and converged to R_1 = 2.67%. The experimental details for aluminosugilite are summarized in Table 2. The refined site occupancies, atomic coordinates, and anisotropic displacement parameters are listed in Table 3, and the selected interatomic distances and angles are given in Table 4. The structural formula for aluminosugilite is represented as $KNa_2(Al_{1.34}M_{0.66})Li_3Si_{12}O_{30}$ (M = Fe + Mn) based on the refined site occupancies, and the determined unit cell parameters are a = 9.9894(7) Å, c = 13.9527(9) Å, and V = 1205.77(14) Å^3. These parameters are in close agreement with the results of the chemical composition analysis and powder X-ray diffraction measurements.

Figure 4 shows the crystal structure of aluminosugilite. The general structural formula for the milarite group minerals is represented as $^{XII}C^{IX}B_2{}^{VI}A_2{}^{IV}(T2)_3{}^{IV}(T1)_{12}O_{30}$, where C = K, B = Na, A = Al, $T2$ = Li, and $T1$ = Si for ideal aluminosugilite. This is a double-ring silicate mineral, where two double-ring units formed by the $T1$ tetrahedra are stacked above each other. The space within the double-ring unit is void, while the C site occupied by K is coordinated in the space between the units. The $T2$ and A sites are located in the same a–b plane as the C site, and these polyhedra are linked to the double-ring units. The $T2$ site is a tetrahedrally coordinated site occupied by Li, where the tetrahedron is larger than the silicate tetrahedron exhibiting a high degree of angular distortion. This Li-centered tetrahedron is connected to the double-ring unit by O3-sharing and the octahedra with the A site by sharing the O3-O3 edge. The A site is occupied by trivalent cations such as Al, Fe, and Mn, which form a regular octahedron. The B site is a 9-coordinated site occupied by Na, located be-

Table 3. Refined atomic coordinates, displacement parameters (Å^2), and site occupancies for aluminosugilite

	x	*y*	*z*	U^{eq}	Occupancy
^{C}K	0	0	1/4	0.0198(3)	$K_{1.0}$
^{B}Na	1/3	2/3	0.0124(9)	0.027(2)	$Na_{0.5}$
^{A}Al	1/3	2/3	1/4	0.00735(19)	$Al_{0.669(5)}Fe_{0.331}$
^{T2}Li	0.5	0.5	1/4	0.0159(10)	$Li_{1.0}$
^{T1}Si	0.23585(5)	0.35795(5)	0.38629(2)	0.00876(10)	$Si_{1.0}$
O1	0.14072(19)	0.3990(2)	0	0.0173(3)	$O_{1.0}$
O2	0.22491(13)	0.27784(14)	0.13808(8)	0.0161(2)	$O_{1.0}$
O3	0.16941(12)	0.51112(12)	0.17128(7)	0.0128(2)	$O_{1.0}$

	U^{11}	U^{22}	U^{33}	U^{12}	U^{13}	U^{23}
^{C}K	0.0186(3)	0.0186(3)	0.0230(5)	0.00931(17)	0	0
^{B}Na	0.0188(6)	0.0188(6)	0.043(6)	0.0094(3)	0	0
^{A}Al	0.0069(2)	0.0069(2)	0.0083(3)	0.00344(12)	0	0
^{T2}Li	0.0158(19)	0.0158(19)	0.019(2)	0.010(2)	0	0
^{T1}Si	0.00818(17)	0.00908(17)	0.00921(17)	0.00447(13)	0.00053(11)	0.00049(12)
O1	0.0212(8)	0.0189(8)	0.0094(6)	0.0082(7)	0	0
O2	0.0148(5)	0.0174(5)	0.0208(5)	0.0117(4)	0.0004(4)	0.0000(4)
O3	0.0116(4)	0.0112(4)	0.0156(4)	0.0056(4)	−0.0010(3)	−0.0034(4)

tween octahedra aligned along the ***c***-axis direction. The displacement parameter for the *B* site is strongly elongated in the ***c***-axis direction in the ordered model. Therefore, the analysis was performed allowing a degree of freedom in the ***c***-axis direction, which improved the *R* factor. In this case, the *B* site is disordered, and the occupancy is 50%, which has been observed in previous studies (Armbruster and Oberhänsli, 1988; Nagashima et al., 2020).

Discussion

Sugilite series minerals are classified according to the priority of the cations that occupy the *A* site located in the octahedral center, with the Fe^{3+}-preferred sugilite being found first (Murakami et al., 1976), and its Al substituent being aluminosugilite (Nagashima et al., 2020). At 6-coordination octahedral sites, the ionic radius of Fe^{3+} is greater than that of Al, and the *A*-O distance also shows harmonic behavior, with that for sugilite being longer than that for aluminosugilite (Table 4). The compositional distribution of the series of minerals from various localities suggests that sugilite and aluminosugilite form a solid solution over a wide range of compositions. In addition, sugilite and aluminosugilite often contain small amounts of Mn^{3+} (Fig. 3). The ionic radii of Fe^{3+} and Mn^{3+} at 6-coordination octahedral sites are the same, and the existence of sugilite close to the Fe^{3+} end-member compositions suggests that a Mn^{3+} analog of sugilite is also possible in terms of ionic radius. However, the amount of Mn^{3+} found in these minerals has been limited to date. The Mn^{3+} content was at most 20% in the Al-Fe-Mn system of aluminosugilite from the Funakozawa mine. Even if Mn^{3+} occurs in Mn deposits from other localities, the amount of Mn^{3+} was generally less than 30% in the Al-Fe-Mn system (Fig. 3). The solubility of Mn^{3+} may be inhibited by factors other than the ionic radius, such as the Jahn-Teller effect of Mn^{3+} cation and the symmetry of the structure. Octahedrally coordinated Mn^{3+} cation is known to induce structural distortion. However, the central cation of the AO_6-octahedron in the sugilite structure bonds to six equivalent O atoms at the O3 sites; therefore, the octahedron has an almost regular shape (Table 4). As long as the structure retains the *P*6/*mcc* space group, there is likely to be an accommodation limit for Mn^{3+}, even if the ionic radius is acceptable for the octahedron. However, if symmetry lowering is possible in the sugilite structure that allows octahedral Jahn-Teller distortion, it may change the upper solubility limit of Mn^{3+}. Although sugilite with the highest Mn^{3+} content found in the Furumiya mine falls into the Mn-dominant region of the Al-Fe-Mn system (Fig. 3), no structural analysis of such Mn-rich samples has been performed. Further investigation of Mn^{3+}-rich samples is thus required to elucidate the details of the sugilite-series minerals.

Aluminosugilite occurred only in a very thin layer in the siliceous slate of the Funakozawa mine. Therefore, the formation of aluminosugilite is probably due to very limited activity. In particular, the only Al-bearing mineral in this layer was aluminosugilite. However, ferri-leakeite is abundant and ubiquitous in the aluminosugilite-bearing

Table 4. Selected interatomic distances (Å) and angles (°) for (alumino)sugilite

Sample	Aluminosugilite		Sugilite	
Reference	1	2	2	3
Al apfu	1.31	1.38	0.36	0.50
Mn^{3+} apfu	0.17	0.31	0.00	0.30
Fe^{3+} apfu	0.44	0.24	1.52	1.12
C-O2 (×12)	2.9922(11)	2.995	2.997	2.994
B-O1 (×3)	2.395(2)	2.394	2.419	2.42
B-O3 (×3)	2.732(11)	2.78	2.75	2.733
B-O3 (×3)	3.020(11)	2.98	3.03	3.088
A-O3 (×6)	1.9385(10)	1.9395	1.981	1.972
O3-*A*-O3	85.97(6)	85.84	85.61	85.73
O3-*A*-O3	91.06(4)	91.09	91.19	91.09
O3-*A*-O3	92.08(6)	92.15	92.18	92.27
*T*2-O3 (×6)	1.9735(10)	1.970	1.972	1.972
O3-*T*2-O3	84.09(6)	84.21	86.1	86.8
O3-*T*2-O3	112.36(6)	112.23	110.8	111
O3-*T*2-O3	136.26(6)	136.28	135.4	135.7
*T*1-O1	1.6259(5)	1.624	1.626	1.625
*T*1-O2	1.6225(12)	1.6207	1.621	1.620
*T*1-O2	1.6172(11)	1.6172	1.619	1.615
*T*1-O3	1.5769(11)	1.5788	1.575	1.577
O1-*T*1-O2	107.94(8)	108.11	108.0	108.1
O1-*T*1-O3	108.15(8)	108.35	108.0	108.0
O2-*T*1-O1	110.6(7)	110.56	111.0	110.8
O2-*T*1-O3	111.51(6)	111.27	111.6	111.4
O2-*T*1-O2	103.97(9)	104.14	103.7	104.0
O3-*T*1-O2	114.54(6)	114.32	114.5	114.4

1, This study; 2, Nagashima et al. (2020); 3, Armbruster and Oberhänsli (1988).

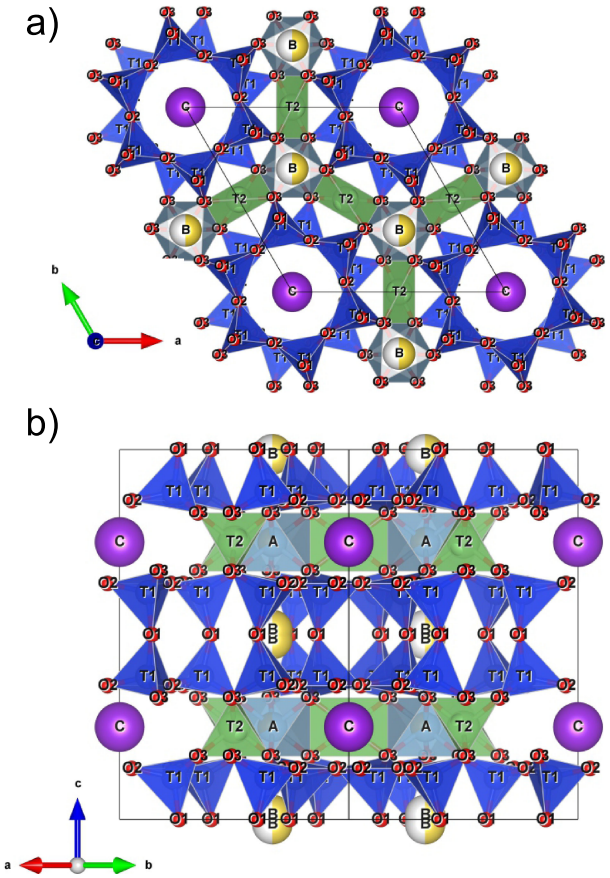

Figure 4. Crystal structure of aluminosugilite along from the (a) [001] and (b) [110] directions using VESTA (Momma and Izumi, 2011). The general structural formula for the milarite group mineral is represented as $^{XII}C^{IX}B_2{}^{VI}A_2{}^{IV}(T2)_3{}^{IV}(T1)_{12}O_{30}$, where C = K, B = Na, A = Al, $T2$ = Li, and $T1$ = Si for ideal aluminosugilite.

rocks, and the elements common to them, such as Li, may have already been satisfied before the formation of aluminosugilite. Aluminosugilite may be a better indicator of Al activity than Li in this locality. Dating based on the K in (alumino)sugilite suggested the age of hydrothermal events that led to the enrichment of Mn deposits at the Wessels and Bruce mines (e.g., Gnos et al., 2003; Moore et al., 2011), but at the Funakozawa mine it would be the aluminum activity age.

NORRISHITE

Appearance

Norrishite is one of the most abundant constituent minerals in slate, and its appearance in the boulder and outcrop samples was the same. Norrishite is not entirely distributed throughout the slate but is concentrated in specific quartz layers. The quartz layer rich in norrishite also contains large amounts of aegirine, amphibole, and braunite (Fig. 5). The norrishite-rich quartz layer is thus brown to black in color and the predominance of quartz is not evident. The norrishite crystal size is often less than 0.5 mm in this quartz layer, but can be up to 1 mm. On the other hand, the other constituent minerals are mostly fine crystals with a size of approximately 10 μm. Therefore, norrishite is the only mineral that is visible to the naked eye on the fracture surface of the slate (Fig. 5a).

Norrishite is in the form of brown, irregularly shaped foil-like to plate-like crystals that exhibit perfect cleavage at {001} planes and has a Mohs hardness of 2.5–3.0. In thin sections, norrishite is surrounded by quartz (Fig. 5b). Pleochroism is strong with color variation from yellow to brown to green. Norrishite occasionally includes minerals distributed in slate, such as aegirine, amphibole, and braunite (Fig. 5c).

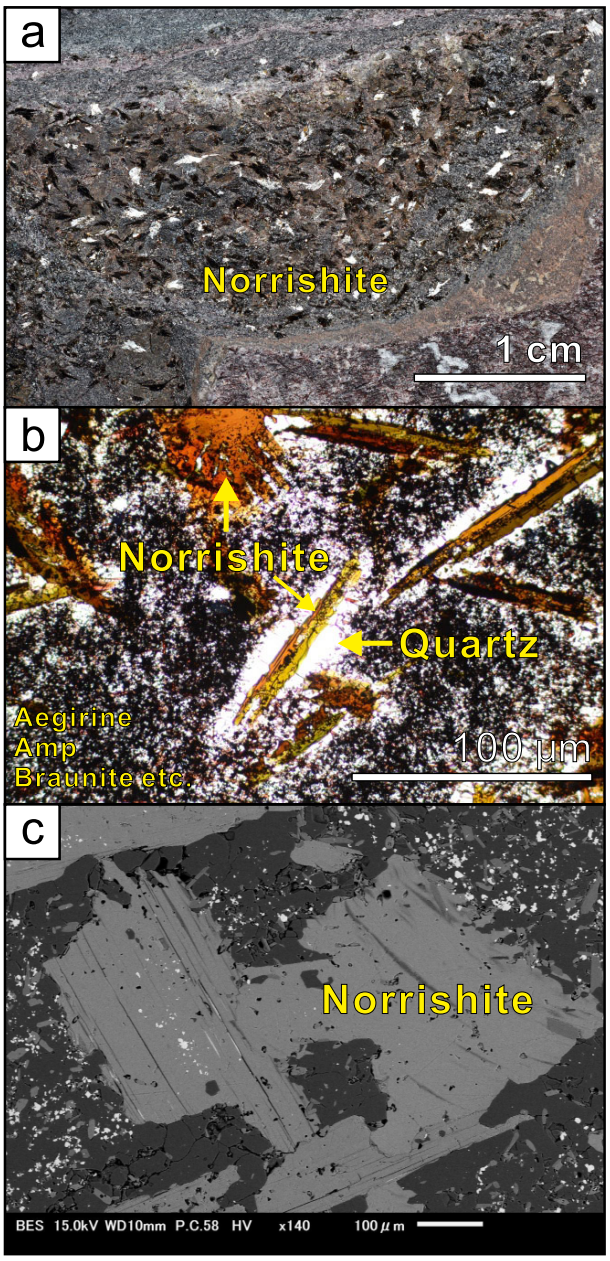

Figure 5. (a) Fracture surface of a quartz layer rich in norrishite, (b) micrograph under polarized light, and (c) backscattered electron image.

Table 5. Chemical composition of norrishite

	Boulder (n = 10)	Outcrop (n = 10)
	wt%	wt%
	Avg. (Min.-Max)	Avg. (Min.-Max)
K_2O	9.74 (9.57-10.00)	9.88 (9.75-10.02)
Mn_2O_3	32.48 (32.08-33.49)	34.07 (33.24-35.30)
MgO	0.73 (0.48-0.88)	0.63 (0.46-0.82)
TiO_2	0.42 (0.24-0.58)	0.28 (0.04-0.42)
Li_2O^*	2.88	2.55
Al_2O_3	2.39 (2.16-2.60)	1.78 (1.26-2.11)
SiO_2	47.47 (46.47-48.51)	47.68 (47.05-48.37)
Total	96.11	96.87
	apfu	apfu
K	0.99	1.01
Mn	1.97	2.08
Mg	0.09	0.07
Ti	0.03	0.02
Li	0.92	0.82
Σ =	3	3
Al	0.22	0.17
Si	3.78	3.83
Σ =	4	4
O	11.95	12.07

* Calculated value from stoichiometry.

Chemical composition

The chemical composition of norrishite was determined for both the boulder and outcrop samples; Table 5 summarizes the chemical composition of these norrishite samples, obtained as the average of 10 analyses for each specimen. Since no OH was detected and the $M1$ site was almost entirely occupied by Li in the single crystal XRD analysis, the empirical formula was calculated on the basis of Si + Al = 4 apfu, and the Li_2O wt% was recalculated by considering the lack of M sites from 3 apfu as Li. On the other hand, it is noted that the total wt% with such an estimate is slightly less than the ideal value. The exact amount of Li and the presence or absence of OH and Mn^{2+} are also issues that need to be investigated in the future. The representative chemical compositions of norrishite are $K_{0.99}(Mn_{1.97}Mg_{0.09}Ti_{0.03}Li_{0.92})_{\Sigma 3}(Al_{0.22}Si_{3.78})_{\Sigma 4}O_{11.95}$ and $K_{1.01}(Mn_{2.08}Mg_{0.07}Ti_{0.02}Li_{0.82})_{\Sigma 3}(Al_{0.17}Si_{3.83})_{\Sigma 4}O_{12.07}$ from the boulder and outcrop samples, respectively. Norrishite has a Fe-free composition, despite coexistence with aegirine and amphiboles such as ferri-leakeite.

Figure 6 shows the variation in the Si and Mn contents of norrishite. The Si content in the Funakozawa norrishite is slightly less than 4.0 apfu, which indicates the presence of a small amount of Al at the tetrahedral sites. The compositions of the two samples are very similar, with only slight differences in the Si and Mn contents.

X-ray crystallography

Powder X-ray diffraction data were measured using the boulder sample. Supplementary Figure S2 shows the powder X-ray diffraction pattern obtained. Although a large amount of quartz is detected due to the close association

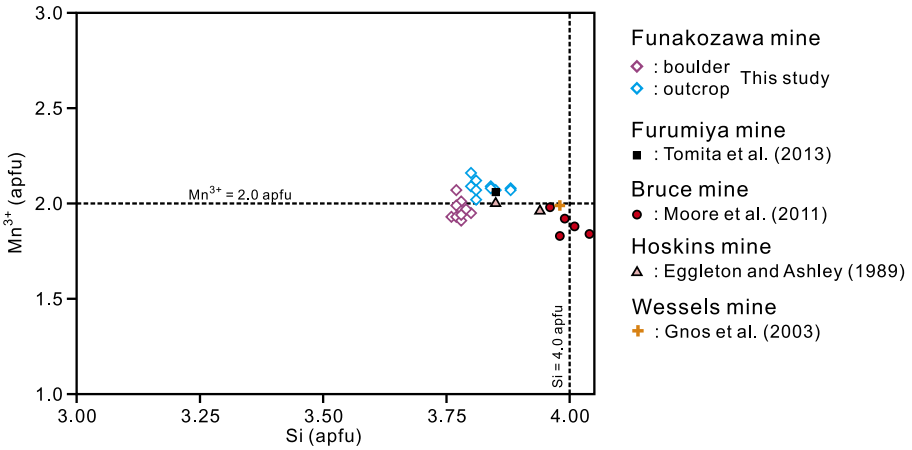

Figure 6. Si and Mn contents of norrishite from the Funakozawa mine and other localities.

Table 6. Refined atomic coordinates, displacement parameters (Å^2), and site occupancies for norrishite

	x	*y*	*z*	U^{eq}	Occupancy
K	0	0	0	0.0268(2)	$K_{1.0}$
*M*1	0	0	0.5	0.0094(10)	$Li_{0.944(4)}Mn_{0.056}$
*M*2	0	0.34736(3)	0.5	0.00841(12)	$Mn_{0.970(3)}$
Si	0.06328(8)	0.17034(5)	0.22658(5)	0.00888(14)	$Si_{1.0}$
O1	0.0461(4)	0	0.16868(19)	0.0142(3)	$O_{1.0}$
O2	0.2967(2)	0.24870(15)	0.16074(13)	0.0131(2)	$O_{1.0}$
O3	0.1092(2)	0.17912(14)	0.38679(13)	0.0102(2)	$O_{1.0}$
O4	0.1095(3)	0.5	0.3972(2)	0.0127(3)	$O_{1.0}$

	U^{11}	U^{22}	U^{33}	U^{12}	U^{13}	U^{23}
K	0.0277(4)	0.0208(4)	0.0319(5)	0	0.0045(3)	0
*M*1	0.0067(14)	0.0066(15)	0.0152(18)	0	0.0030(10)	0
*M*2	0.00735(16)	0.00579(15)	0.01218(18)	0	0.00165(10)	0
Si	0.00711(19)	0.00691(19)	0.0125(2)	0.00003(11)	0.00106(14)	−0.00020(12)
O1	0.0177(7)	0.0079(6)	0.0166(8)	0	0.0013(6)	0
O2	0.0097(4)	0.0154(5)	0.0142(5)	−0.0040(4)	0.0016(3)	−0.0002(4)
O3	0.0092(4)	0.0088(4)	0.0124(5)	0.0005(3)	0.0008(3)	−0.0007(3)
O4	0.0140(6)	0.0076(6)	0.0174(8)	0	0.0055(5)	0

with norrishite, the diffraction peaks associated with norrishite could be well identified. The overall diffraction profile is very compatible with the *M*1-polytype structure. The unit cell parameters were refined with the space group *C*2/*m* using 47 peaks indexed in the *d* = 9.98–1.52 Å range, which gave *a* = 5.3011(5) Å, *b* = 8.94525(10) Å, *c* = 10.0789(9) Å, *β* = 98.276(9)°, and *V* = 472.96(8) Å^3. Supplementary Table S2 summarizes the powder X-ray diffraction data for norrishite.

Structure refinement was performed using single-crystal X-ray diffraction data for the boulder sample. The diffraction spots did not show any obvious indication of twinning, stacking faults, or polymorphism, and the structure could thus be fully analyzed as a 1*M* type structure with space group *C*2/*m*. The refinement converged to R_1 = 4.30%, and the determined unit cell parameters were *a* = 5.3024(2) Å, *b* = 8.9520(4) Å, *c* = 10.0812(5) Å, *β* = 98.191(4)°, and *V* = 473.65(4) Å^3. The experimental details are summarized in Table 2. The refined site occupancies, atomic coordinates and anisotropic displacement parameters are listed in Table 6, and the selected interatomic distances and angles are given in Table 7.

Figure 7 shows the crystal structure of norrishite. The general structural formula for the mica group mineral is represented as $IM_{2\text{-}3}T_4O_{10}A_2$, and the ideal formula for norrishite is shown as $KLiMn_2^{3+}Si_4O_{10}O_2$. Norrishite is a trioctahedral mica, and its structure consists of one octahedral sheet containing Li and Mn and two opposing silicate tetrahedral sheets. These sheets form a layer that is separated from adjacent layers by a plane of interlayer K cations. The features within the octahedral sheet are described below.

Table 7. Selected interatomic distances (Å) and angles (°) for norrishite

Reference	1	2
*M*1 (occ.)	$Li_{0.944}Mn_{0.056}$	$Li_{1.0}$
*M*2 (occ.)	$Mn_{0.970}$	$Mn_{1.0}$
T (apfu)	$Si_{3.78}Al_{0.22}$	$Si_{3.94}Al_{0.06}$
K-O1 (×2)	3.139(3)	3.12
K-O1 (×2)	3.142(2)	3.12
K-O2 (×2)	3.0401(14)	3.029
K-O2 (×2)	3.0717(13)	3.064
*M*1-O3 (×4)	2.0970(13)	2.092
*M*1-O4 (×2)	2.1794(16)	2.18
Mean	2.124	2.121
O3-*M*1-O3 (×2)	80.25(8)	80.8
O3-*M*1-O4 (×4)	86.65(5)	86.9
O3-O3 (×2)*	3.207(3)	3.19
O3-O4 (×4)*	3.1116(19)	3.10
O3-*M*1-O3 (×2)*	99.75(8)	99.2
O3-*M*1-O4 (×4)*	93.35(5)	93.1
*M*2-O3 (×2)	2.0235(14)	2.023
*M*2-O3′ (×2)	2.2313(11)	2.223
*M*2-O4 (×2)	1.8573(14)	1.855
Mean	2.037	2.037
O3-*M*2-O3	83.80(8)	84.1
O3-*M*2-O3′ (×2)	83.68(5)	84.2
O4-*M*2-O3′ (×2)	91.27(6)	91.4
O4-*M*2-O4	85.27(10)	85.5
O3-O3′ (×2)*	2.9393(11)	2.93
O3-O4 (×2)*	2.8744(13)	2.87
O4-O3′ (×2)*	3.0887(18)	3.08
O3-*M*2-O3′ (×2)*	87.25(5)	87.0
O3-*M*2-O4 (×2)*	95.48(6)	95.1
O4-*M*2-O3′ (×2)*	97.71(6)	97.3
*T*1-O1	1.6307(9)	1.633
*T*1-O2′	1.6427(14)	1.638
*T*1-O2	1.6421(12)	1.636
*T*1-O3	1.6006(14)	1.571
O1-*T*1-O2′	105.16(10)	104.8
O1-*T*1-O2	105.49(9)	105.2
O1-*T*1-O3	113.57(9)	113.8
O2-*T*1-O2′	107.63(6)	108.1
O2-*T*1-O3	112.62(7)	111.7
O2′-*T*1-O3	111.82	112.6

* Unshared edge

1, this study; 2, Tyrna and Guggenheim (1991)

The octahedral sheet consists of two *M* sites occupied by Li and Mn^{3+} (Fig. 7b). They are also almost completely ordered as Li at the *M*1 sites and Mn^{3+} at the *M*2 sites

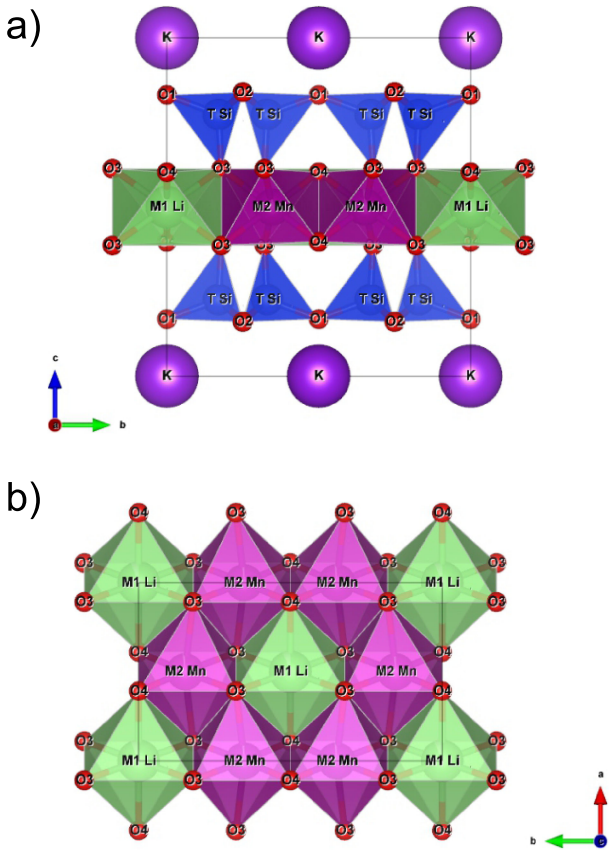

Figure 7. Crystal structure of norrishite and its octahedral sheet drawn along the (a) [100] and (b) [001] directions using VESTA (Momma and Izumi, 2011).

(Table 6). Li and Mn^{3+} have different ionic radii and electron orbitals, so that the size and shape of each octahedron are also different. The octahedron with the *M*1 site for Li is close to a regular shape, and the *M*1-O bond lengths are also close to each other. The mean *M*1-O bond length is slightly larger than the mean *M*2-O bond length, making the *M*1 site suitable for accommodating Li with a large ionic radius. The shorter *M*2-O bonds are ideal for accommodating Mn^{3+} with a small ionic radius. Furthermore, the attraction between *M*2 and O4 caused by the presence of O instead of OH at the O4 site results in a shorter *M*2-O4 bond and the formation of an environment that is preferentially occupied by the Jahn-Teller cation, Mn^{3+}. Thus, Li and Mn occupy one of the two *M* sites based on their ionic size, electronic character, and structural flexibility. The atomic coordinates and bond lengths measured for norrishite were not significantly different from those reported by Tyrna and Guggenheim (1991) (Table 7).

Discussion

The composition of norrishite from five localities has been

reported (Fig. 6). The variation in the Si and Mn contents is very small across all localities. Norrishite is always close to the end-member composition, regardless of the source. For example, the range of Mn^{3+} content is small, within approximately 2.0 ± 0.2 apfu in any of the examined localities. This is equal to the value when Mn^{3+} occupies the M2 sites. Single-crystal structural analysis has confirmed the presence of Mn^{3+} at the M2 sites, and the same phenomenon probably occurs in other occurrences of norrishite. Norrishite from all localities is also typically poor in sub-components and has almost exclusivity a Fe-free composition. Tyrna and Guggenheim (1991) suggested that the lack of Fe^{3+} in norrishite was due to its absence in the surrounding environment, although Gnos et al. (2003) reported the occurrence of norrishite coexisting with Fe^{3+}-containing minerals. Although the Funakozawa norrishite also coexists with Fe^{3+}-bearing minerals such as aegirine and ferri-leakeite, Fe was undetectable (Table 5). Fe^{3+} is probably rejected from the structural environment of norrishite despite having the same ionic radius as Mn^{3+}. The octahedron with Mn is significantly distorted by its own Jahn-Teller effect, which makes it an environment occupied only by itself. Therefore, it cannot accept Fe^{3+} and other cations, and subsequently the octahedron containing Li cannot accept other cations. Although Na is also present in the environment, it cannot be substituted for K and/or Li in norrishite, because of the significant difference in ionic radius. Norrishite is the only Mn^{3+}-dominant species in the mica group. The structure is sufficiently flexible to accept the Jahn-Teller cation, Mn^{3+}, but once it is accepted, the solid solution that can be formed is considered to be quite limited. However, it may be possible to accommodate small amounts of Li-Mn disorder and other elements (Mg and Ti). Norrishite from the Funakozawa mine has the most Si-poor (Al-rich) composition to date, and its electronic neutralization is considered to be counterbalanced within the octahedral sheets (Tables 5 and 6).

Norrishite is one of the most abundant constituent minerals in the Funakozawa mine, both in outcrops and boulders. Nambu (1980) classified the Funakozawa mine in the biotite zone, where biotite is probably norrishite at this location. These ubiquitous minerals can be dated; Gnos et al. (2003) derived crystallization and alteration ages for norrishite by Ar dating. The age of active Li addition would also be recorded in norrishite in the Funakozawa mine because it is not a temporary vein mineral but a common mineral. Norrishite and Li-bearing amphiboles (ferri-leakeite) have also been described from the host rock of the Kotamagawa mine, which is located 4 km north-west of the Funakozawa mine (Nishio-Hamane et al., 2023). The very widespread and common distribution of Li-containing minerals has not been fully understood until now. Along with the mineralogical features of norrishite identified here, the geochemical characteristics will also be important to elucidate the Li resources of this region.

CONCLUSION

Descriptive mineralogical studies, including single-crystal structure analysis, were conducted on aluminosugilite and norrishite, two scarce minerals from the Funakozawa mine. Aluminosugilite is characterized by a high Al content at octahedral sites, with a wide distribution between Al-Fe, but limited to low Mn content. This is interpreted to be due to the symmetry of the structure, which does not allow the octahedron to be distorted in one direction and cannot accommodate large amounts of Mn^{3+}, the Jahn-Teller cation. On the other hand, the mica structure is sufficiently flexible to accept Mn^{3+}, although when incorporated, the formation of a solid solution with other components becomes limited. As a result, norrishite is close to an ideal composition, although there is a small amount of Si-Al substitution.

The formation of aluminosugilite is very limited in the Funakozawa mine and its occurrence would be a good indicator of Al activity rather than Li. Norrishite, as with Li-bearing amphibole, is a common mineral in the area and is thus a good indicator of Li activity. The vast and ubiquitous distribution of Li-containing minerals has been poorly understood to date. In addition to the mineralogical characteristics of the minerals revealed in this study, geochemical properties will also be critical in the identification of Li resources.

ACKNOWLEDGMENTS

One of the authors (MN) thanks Yoji Morifuku (Centre of Instrumental Analysis, Yamaguchi University) for technical assistance, and gratefully acknowledges the financial support of a Grant-in-Aid for Scientific Research (No. JP23K03551) from the Japan Society for the Promotion of Science (JSPS). This study employed research equipment shared in the Ministry of Education, Culture, Sports, Science and Technology (MEXT) Project for Promoting Public Utilization of Advanced Research Infrastructure (Program for supporting construction of core facilities, Grant no. JPMXS040040023) and was also supported by the Core Clusters for Research Initiative of Yamaguchi University. Synchrotron radiation X-ray powder diffraction experiments were performed at SPring-8 with the approval of the Japan Synchrotron Radiation Research Institute (JASRI) (Proposal No. 2023A2372).

SUPPLEMENTARY MATERIALS

Supplementary Figures S1–S2, Tables S1–S2 and Supplementary CIF files are available online from https://doi.org/10.2465/jmps.240509.

REFERENCES

Armbruster, T. and Oberhänsli, R. (1988) Crystal chemistry of double-ring silicates: Structures of sugilite and brannockite. American Mineralogist, 73, 595–600.

Armbruster, T., Oberhänsli, R. and Kunz, M. (1993) Taikanite, $BaSr_2Mn_2^{3+}O_2[Si_4O_{12}]$, from the Wessels mine, South Africa: a chain silicate related to synthetic $Ca_3Mn_2^{3+}O_2[Si_4O_{12}]$. American Mineralogist, 78, 1088–1095.

Cabella, R., Lucchetti, G. and Palenzona, A. (1990) Al-rich, Fe-poor manganoan sugilite in a pectolite-bearing assemblage from Cerchiara Mine (Northern Appennines, Italy). Neues Jahrbuch für Mineralogie, Monatshefte, 10, 443–448.

Dixon, R.D. (1989) Sugilite and associated metamorphic silicate minerals from Wessels Mine, Kalahari manganese field. Bulletin of the Geological Survey of South Africa, 92, 1–47.

Dunn, P.J., Brummer, J.J. and Belsky, H. (1980) Sugilite, a second occurrence: Wessels mine, Kalahari manganese field, Republic of South Africa. The Canadian Mineralogist, 18, 37–39.

Eggleton, R.A. and Ashley, P.M. (1989) Norrishite, a new manganese mica, $K(Mn_2^{3+}Li)Si_4O_{12}$, from the Hoskins mine, New South Wales, Australia. American Mineralogist, 74, 1360–1367.

Gnos, E., Armbruster, T. and Villa, I.M. (2003) Norrishite, $K(Mn_2^{3+}Li)Si_4O_{10}(O)_2$, an oxymica associated with sugilite from the Wessels Mine, South Africa: Crystal chemistry and 39Ar-40Ar dating. American Mineralogist, 88, 189–194.

Gu, X., Yang, H., Xie, X., Van Nieuwenhuizen, J., et al. (2019) Lipuite, a new manganese phyllosilicate mineral from the N'Chwaning III mine, Kalahari Manganese Fields, South Africa. Mineralogical Magazine, 83, 645–654.

Hawthorne, F.C., Oberti, R., Cannilo, E., Sardone, N., et al. (1995) A new anhydrous amphibole from the Hoskins mine, Grenfall, New South Wales, Australia: description and crystal structure of ungarettite, $NaNa_2(Mn_2^{2+}Mn_3^{3+})Si_8O_{22}O_2$. American Mineralogist, 80, 165–172.

Hirowatari, F. and Fukuoka, M. (1988) Some problems of the studies on the manganese minerals in Japan. Journal of the Mineralogical Society of Japan, 18, 347–365 (in Japanese with English abstract).

Kato, T., Miura, Y. and Murakami, N. (1976) Crystal structure of sugilite. Mineralogical Journal, 8, 184–192.

Kawachi, Y., Ashley, P.M., Vince, D. and Goodwin, M. (1994) Sugilite in manganese silicate rocks from the Hoskins mine and Woods mine, New South Wales, Australia. Mineralogical Magazine, 58, 671–677.

Kawaguchi, S., Takemoto, M., Osaka, K., Nishibori, E., et al. (2017) High-throughput powder diffraction measurement system consisting of multiple MYTHEN detectors at beamline BL02B2 of SPring-8. Review of Scientific Instruments, 88, 085111.

Matsumoto, T., Yamano, Y., Sato, T., Ferrara, J.D., et al. (2021) "What is this?" a structure analysis tool for rapid and automated solution of small molecule structures. Journal of Chemical Crystallography, 51, 438–450.

Momma, K. and Izumi, F. (2011) VESTA 3 for three-dimensional visualization of crystal, volumetric and morphology data. Journal of Applied Crystallography, 44, 1272–1276.

Moore, J.M., Kuhn, B.K., Mark, D.F. and Tsikos, H. (2011) A sugilite-bearing assemblage from the Wolhaarkop breccia, Bruce iron-ore mine, South Africa: Evidence for alkali metasomatism and ^{40}Ar–^{39}Ar dating. European Journal of Mineralogy, 23, 661–673.

Murakami, N., Kato, T., Miúra, Y. and Hirowatari, F. (1976) Sugilite, a new silicate mineral from Iwagi Islet, Southwest Japan. Mineralogical Journal, 8, 110–121.

Nagashima, M., Fukuda, C., Matsumoto, T., Imaoka, T., et al. (2020) Aluminosugilite, $KNa_2Al_2Li_3Si_{12}O_{30}$, an Al analogue of sugilite, from the Cerchiara mine, Liguria, Italy. European Journal of Mineralogy, 32, 57–66.

Nambu, M. (1980) Genesis and problems of the bedded manganese deposits and the bedded manganiferous iron deposits in the Kitakami mountainland, northeastern Japan. Mining Geology, 30, 323–343 (in Japanese with English abstract).

Nambu, M., Tanida, K. and Kita, T. (1969) Kôzulite, a new alkali amphibole from Tanohata Mine, Iwate Prefecture, Japan. Journal of the Japanese Association of Mineralogists, Petrologists and Economic Geologists, 62, 311–328.

Nishio-Hamane, D., Suzuki, Y., Ohki, Y., Ishibashi, T. and Shimobayashi, N. (2022) Aluminosugilite, cerchiaraite-(Mn), and ferri-leakeite from the Funakozawa mine, Iwate Prefecture, Japan. 2022 Annual Meeting of Japan Association of Mineralogical Sciences, R1P-10 (in Japanese with English abstract).

Nishio-Hamane, D., Nagashima, M. and Suzuki, Y. (2023) Norrishite from the Funakozawa mine and Kotamagawa mine, Iwate Prefecture, Japan. 2023 Annual Meeting of Japan Association of Mineralogical Sciences, R1P-10 (in Japanese with English abstract).

Oberti, R., Boiocchi, M., Hawthorne, F.C., Ball, N.A. and Ashley, P.M. (2016) Oxo-mangani-leakeite from the Hoskins mine, New South Wales, Australia: occurrence and mineral description. Mineralogical Magazine, 80, 1013–1021.

Sheldrick, G.K. (2015) Crystal structure refinement with SHELXL. Acta Crystallographica, C71, 3–8.

Suzuki, Y. (2023) Swinefordite, a decomposed mineral from aluminosugilite from the Funakozawa mine, Iwate Prefecture. Kobutsu Joho Mineral Information of Japan, 216, 6–7 (in Japanese).

Tomita, N., Minakawa, T. and Nishio-Hamane, D. (2013) Sr rich K-richterite, fresnoite and norrishite from the Furumiya deposit, Ehime Prefecture, Japan. 2013 Annual Meeting of Japan Association of Mineralogical Sciences, R1-P12 (in Japanese).

Tyrna, P.L. and Guggenheim, S. (1991) The crystal structure of norrishite, $KLiMn_2^{3+}Si_4O_{12}$, and oxygen-rich mica. American Mineralogist, 76, 266–271.

Yoshida, T., Yoshii, M., Katada, M., Takana, K., et al. (1985) Geology of Rikuchu-Ono district. With Geological sheet map at 1:50,000. Geological Survey of Japan, pp. 70 (in Japanese with English abstract).

Yoshii, M., Aoki, Y. and Maeda, K. (1972) Nambulite, a new lithium- and sodium-bearing manganese silicate from the Funakozawa mine, northeastern Japan. Mineralogical Journal, 7, 29–44.

Manuscript received May 9, 2024
Manuscript accepted August 4, 2024
Advance online publication August 20, 2024
Released online publication September 13, 2024
Manuscript handled by Norimasa Shimobayashi